Drivetrain-Integrated Combinatory AC–DC Charging of Electric Vehicles Using an ANFIS-Based DC-Link Controller

Mr. V.Amarnath Reddy[1], B.Madhu Sudhan Reddy[2], G.Sai Charan[3], R.Jagadeeshwar Reddy[4], M.Suresh[5]

[1]Assistant Professor, Department of EEE, AITS, Kadapa

[2,3,4,5]Student (UG), Department of EEE, AITS, Kadapa

Abstract— A major component in accelerating the broad adoption of electric vehicles (EVs) is a decrease in the time it takes to charge their batteries. The upfront and ongoing expenses of commercial off-board high-power DC fast-charging stations are rather substantial, whereas the typical on-board Type-1 and Type-2 AC chargers, with ratings ranging from 3.3 kW to 19 kW, need lengthy charging times. This research suggests a method to charge electric vehicle batteries faster using a combination of AC and DC currents. The suggested method allows for the use of both the on-board Type-2 AC charger and the drivetrain-integrated DC charger to charge the electric vehicle's battery at the same time. Using the neutral point (N) of the EV motor windings and the negative rail (O) of the drivetrain inverter, a DC input port (N(+), O(−)) is created for drivetrain-integrated DC charging. This DC input connector may receive electricity from DC microgrids that are based on renewable energy, solar roofs, and other electric vehicle batteries. By repurposing the motor windings as filter inductors, the electric vehicle's drivetrain inverter may be operated as an integrated interleaved DC-DC converter (IDC). In place of the traditional PI controller, an ANFIS-based DC-link voltage controller is suggested to guarantee adaptive and robust functioning while both AC and DC charging are occurring at the same time. The suggested controller regulates the common DC-link voltage while efficiently handling nonlinearities in the system and fluctuations in source and load circumstances. Through finite element method (FEM) co-simulation using ANSYS Maxwell and Simplorer, the performance of the electric vehicle motor and drivetrain-integrated DC charger is validated with the suggested ANFIS-based control system. In addition, a scaled experimental prototype is created to confirm that the combined AC-DC charging strategy is feasible and practical.

Keywords: Electric vehicles, combinatory AC–DC charging, drivetrain-integrated charger, integrated DC–DC converter, DC-link voltage control, adaptive neuro-fuzzy inference system (ANFIS), onboard charger, DC microgrid.

I. INTRODUCTION

Increasing environmental concerns, strict pollution restrictions, and breakthroughs in battery and power electronic technology are driving the fast expansion of electric vehicles (EVs). One of the key obstacles to widespread EV adoption, even with these advancements, is the lengthy time it takes to charge the batteries [1] – [3]. Therefore, it is crucial to do research on ways to shorten charging times without drastically raising system costs or infrastructural complexity. Two main types of conventional electric vehicle charging

infrastructure exist: on-board AC chargers and off-board DC fast chargers. Despite its ability to offer charging power surpassing 50 kW, high-power off-board DC fast-charging stations are not widely used because to their high maintenance costs, large initial investment, and the need to reinforce the utility grid [4]. On the other hand, electric vehicles with big battery packs require longer charging times when using on-board AC chargers, which are both affordable and widely accessible (Type-1 and Type-2 chargers with ratings between 3.3 kW and 19 kW) [5]. There has been a rise in interest in drivetrain-integrated charging technologies as a means to circumvent these restrictions. These methods allow for higher charging power levels while reducing hardware redundancy, weight, and cost by reusing existing drivetrain components, such as the motor windings and traction inverter [6]-[9]. Using the motor windings as filter inductors, many investigations have shown that the traction inverter may be operated as a bidirectional DC-DC or AC-DC converter when in charging modes [11]. While there are drivetrain-integrated chargers on the market, the vast majority of them can only charge in one of two modes: AC or DC. Direct DC charging of EVs has also become more feasible due to the proliferation of DC microgrids and renewable energy sources. Avoiding numerous rounds of AC-DC conversion can greatly enhance charging efficiency when using DC sources based on renewable energy, such as energy storage systems, vehicle-to-vehicle (V2V) power transmission, and solar roofs [12]. For these DC sources to be used efficiently, charging structures need to be flexible enough to take power from numerous sources at once. This study presents a hybrid AC-DC charging system that allows electric vehicle batteries to be charged using both the on-board Type-2 AC charger and a DC charger that is built into the drivetrain both at once. By connecting the EV motor windings' neutral point with the drivetrain inverter's negative rail, a new DC input port is created, enabling direct connection to external DC sources such DC microgrids and renewable power systems. By converting the electric vehicle's drivetrain inverter into an integrated interleaved DC-DC converter (IDC) and using the motor windings as filter inductors, extra passive components may be omitted. Managing the shared DC-link voltage in the face of nonlinear system dynamics and fluctuating source and load circumstances is a significant obstacle to the efficient functioning of combined AC-DC charging systems. Under these circumstances, traditional proportional-integral (PI) controllers are not very resilient and need to be fine-tuned often [13]. To solve this problem, this study suggests a DC-link voltage controller based on an adaptive neuro-fuzzy inference system (ANFIS). The ANFIS controller effectively handles system nonlinearities and parameter variations[14] - [18] by integrating the learning and reasoning abilities of neural networks with fuzzy logic, which results in adaptive and resilient performance. Through finite element method (FEM) co-simulation using ANSYS Maxwell and Simplorer, we evaluate the efficacy of the proposed combinatory charging architecture and ANFIS-based control scheme [19]. This ensures correct modeling of electromagnetic and power electronic interactions. In addition, we build a scaled experimental prototype to

show how well the system works when charged with both AC and DC power sources at the same time.

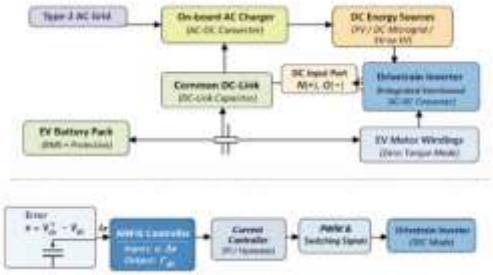


Fig. 1. Drivetrain integrated on-board EV charger configurations of the proposed System.

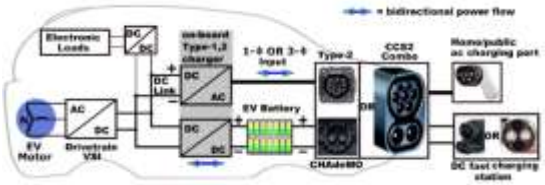


Fig. 2. Power architecture showing drive train, EV motor, on-board power converters with power input ports of an EV.

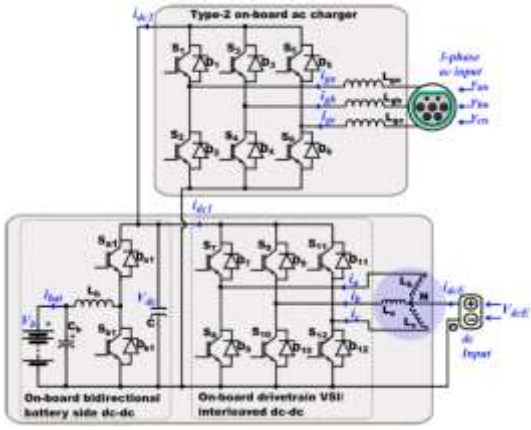


Fig. 3. Detailed circuit diagram of the proposed combinatory ac and dc charging approach.

II. TOPOLOGY OF THE PROPOSED COMBINATORY AC–DC EV CHARGING SYSTEM

The topology of the proposed combinatory AC and DC EV charging system is illustrated in Fig. 3. The proposed configuration enables simultaneous utilization of conventional on-board AC charging infrastructure and an additional drivetrain-integrated DC charging interface, without introducing significant additional hardware. A typical EV passenger car power architecture consists of an on-board Type-1 or Type-2 AC charger, a high-power drivetrain inverter, an EV motor, a battery-side DC–DC converter, and the traction battery pack, as shown in Fig. 2. The on-board AC charger accepts power from a single-phase or three-phase AC grid through the Type-2 inlet and delivers regulated DC power to the common DC-link of the drivetrain. For high-power DC fast charging, the battery terminals are externally accessible through a CHAdeMO or CCS2 Combo port. In most commercial EVs, the CCS2 Combo port integrates both the Type-2 AC and DC fast-charging interfaces into a single inlet. In the proposed topology, in addition to the existing AC and DC charging ports, a **new DC input port (N(+), O(−))** is introduced. The positive terminal of this port, N(+), is derived from the neutral point of the EV motor stator windings, while the negative terminal, O(−), is connected to the negative rail of the drivetrain inverter DC bus. This configuration allows direct interfacing of external DC sources—such as solar rooftop systems, DC microgrids, stationary energy storage systems, and other EV batteries—with the EV drivetrain. The drivetrain inverter is reconfigured during charging operation to function as a **three-legged interleaved DC–DC converter (IDC)**. The stator windings of the EV motor are reutilized as interleaved filter inductors, thereby eliminating the need for additional passive components. Each inverter leg operates with appropriate gating signals to achieve

interleaved boost conversion from the DC input port voltage $V_{dcE}$to the common DC-link voltage. This reuse of drivetrain components significantly improves power density and reduces system cost and weight.

The proposed topology supports three distinct charging modes:

1. **AC-only charging**, where the EV battery is charged exclusively through the on-board Type-2 AC charger.
2. **DC-only charging**, where the EV battery is charged from an external DC source through the drivetrain-integrated IDC via the DC input port.
3. **Combined AC–DC charging**, where both the on-board AC charger and the integrated IDC operate simultaneously to deliver higher charging power to the battery.

In the proposed system, the DC-link is common to the output of the three-phase active rectifier of the on-board AC charger, the drivetrain-integrated IDC, and the battery-side DC–DC converter. The battery-side DC–DC converter, which supports bidirectional power flow, is responsible for regulating the DC-link voltage to its rated value while transferring the combined charging power to the battery pack. Maintaining a stable DC-link voltage is critical to prevent circulating currents between the AC charger output and the IDC output during combined charging operation. The IDC operates in boost mode to elevate the DC input port voltage $V_{dcE}$to the DC-link voltage level. To ensure safe operation, V_{dcE}must remain lower than the rated DC-link voltage; otherwise, the antiparallel diodes of the inverter switches (D7, D9, and D11) may become forward biased, leading to uncontrolled rise in DC-link voltage. In typical EV drivetrains, the DC-link voltage exceeds 600 V, allowing a wide permissible DC input voltage range from approximately 150 V to 500 V. This wide voltage compatibility enables effective utilization of DC sources such as solar photovoltaic systems, DC microgrids, energy storage systems, and vehicle-to-vehicle (V2V) energy sharing platforms. In particular, V2V energy sharing schemes, such as the cooperative framework presented in [22], require flexible, high-power DC interfaces. The proposed DC input port and drivetrain-integrated IDC provide a suitable solution for accepting power from other EV batteries operating in the 350 V to 450 V range, enabling faster and more flexible EV charging.

III. CONTROL METHODOLOGY

The proposed combinatory AC–DC EV charging system employs a hierarchical control strategy to ensure stable DC-link voltage regulation, coordinated power sharing between multiple sources, and safe battery charging under varying operating conditions. The overall control structure consists of three primary control layers: (i) on-board Type-2 AC charger control, (ii) drivetrain-integrated interleaved DC–DC converter (IDC) control, and (iii) battery-side DC–DC converter control.

A. On-Board AC Charger Control

The on-board Type-2 AC charger consists of a three-phase active front-end (AFE) rectifier connected to the AC grid. The AFE operates under unity power factor control using a synchronous reference frame (SRF) current control strategy. The primary control objectives of the AFE are:

1. Regulation of AC-side currents to follow their references.
2. Maintenance of unity power factor at the grid interface.

3. Delivery of regulated DC power to the common DC-link.

The outer voltage control loop generates the DC-link current reference, while the inner current control loop ensures fast tracking of the reference currents. During combined AC–DC charging operation, the AFE contributes a portion of the required DC-link power based on grid availability and charger rating.

B. Drivetrain-Integrated Interleaved DC–DC Converter Control

During DC charging operation, the drivetrain inverter is reconfigured as a three-phase interleaved boost DC–DC converter. Each inverter leg operates with a phase-shifted pulse-width modulation (PWM) strategy, resulting in interleaved inductor currents through the motor stator windings. This interleaving significantly reduces input current ripple and DC-link voltage ripple. The primary control objective of the IDC is to regulate the power drawn from the external DC source connected at the DC input port V_{dcE}. The IDC operates in current-controlled mode, where the reference current is generated based on the DC-link voltage regulation requirement. The duty cycle of each inverter leg is adjusted to control the average inductor current and hence the power transferred to the DC-link.

C. Battery-Side DC–DC Converter and DC-Link Regulation

The battery-side DC–DC converter is bidirectional and operates as a boost converter during drive mode and as a buck converter during charging mode. In the proposed system, this converter is responsible for regulating the DC-link voltage to its reference value V_{dc}^{*}under all charging scenarios. During combined AC–DC charging, the battery-side DC–DC converter absorbs the total charging power supplied by both the AFE rectifier and the IDC. The controller ensures smooth power flow into the battery while maintaining a stable DC-link voltage and preventing circulating currents between the charging sources.

D. ANFIS-Based DC-Link Voltage Controller

To address the nonlinear dynamics and parameter variations inherent in the combined charging system, an Adaptive Neuro-Fuzzy Inference System (ANFIS)–based controller is employed for DC-link voltage regulation. The conventional PI controller is replaced by the ANFIS controller in the outer voltage control loop of the battery-side DC–DC converter. The ANFIS controller uses the DC-link voltage error $e(k) = V_{dc}^{*} - V_{dc}(k)$and the change in error $\Delta e(k)$as its input variables. Based on a set of fuzzy inference rules and adaptive learning algorithms, the ANFIS controller generates the reference current for the battery-side DC–DC converter. This adaptive control structure enables robust DC-link regulation under rapid changes in AC and DC source availability, load conditions, and system nonlinearities.

IV. MATHEMATICAL ANALYSIS OF THE PROPOSED CHARGING SYSTEM

A. Mathematical Model of the Integrated Interleaved DC–DC Converter

During DC charging operation, each inverter leg of the drivetrain inverter operates as a boost converter. The motor stator windings act as filter inductors with inductance $L_s$and resistance R_s. The averaged state-space equations of a single IDC phase can be expressed as

$$L_s \frac{di_L}{dt} = d\,V_{dcE} - (1-d)\,V_{dc}$$

$$C_{dc}\frac{dV_{dc}}{dt} = \sum_{k=1}^{3}(1-d_k)i_{Lk} + i_{AFE} - i_{bat}$$

where $d$is the duty ratio of the inverter leg, $i_L$is the inductor current, $V_{dcE}$is the external DC input voltage, $V_{dc}$is the DC-link voltage, $C_{dc}$is the DC-link capacitance, $i_{AFE}$is the current contributed by the AC charger, and $i_{bat}$is the battery charging current.

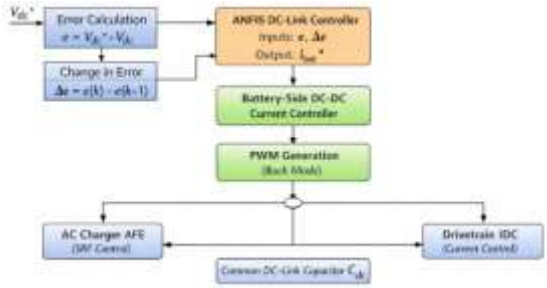


Fig. 4. Control block diagram of the proposed combinatory AC–DC EV charging system with ANFIS-based DC-link voltage regulation.

Due to interleaved operation with 120° phase shift between inverter legs, the net DC-link current ripple is significantly reduced, improving overall system performance.

B. DC-Link Voltage Dynamics

The DC-link voltage dynamics are governed by the net power balance at the DC-link. The instantaneous power balance can be expressed as

$$P_{AFE} + P_{IDC} = P_{bat} + P_{loss}$$

Neglecting losses for control-oriented analysis, the DC-link voltage dynamics can be approximated as

$$C_{dc}V_{dc}\frac{dV_{dc}}{dt} = V_{dc}(i_{AFE} + i_{IDC} - i_{bat})$$

Equation (4) highlights the nonlinear relationship between the DC-link voltage and the charging currents, which motivates the use of an adaptive control approach.

C. Battery-Side DC–DC Converter Model

During charging mode, the battery-side DC–DC converter operates in buck mode. The averaged inductor current dynamics are given by

$$L_b\frac{di_b}{dt} = d_bV_{dc} - V_{bat}$$

$$C_b\frac{dV_{bat}}{dt} = i_b - i_{load}$$

where $L_b$is the battery-side inductance, $d_b$is the duty ratio of the battery-side converter, $V_{bat}$is the battery voltage, and $i_{load}$is the battery charging current.

D. ANFIS-Based DC-Link Control Law

The ANFIS controller maps the nonlinear relationship between the DC-link voltage error and the required battery-side current reference. The control law can be expressed as

$$i_{bat}^{*} = f_{ANFIS}(e, \Delta e)$$

where $f_{ANFIS}(\cdot)$represents the nonlinear mapping implemented by the trained ANFIS network. By adaptively tuning the membership functions and rule parameters, the controller ensures fast dynamic response and robust DC-link voltage regulation under combined AC–DC charging operation.

V. RESULTS

The proposed combinatory AC and DC EV charging system is simulated in MATLAB/Simulink using the parameters listed in Table II. The performance of the system under AC-only, DC-only, and combined AC–DC charging modes is evaluated, with particular emphasis on the effectiveness of the proposed ANFIS-based DC-link voltage controller.

Case1: Type-2 AC Charging

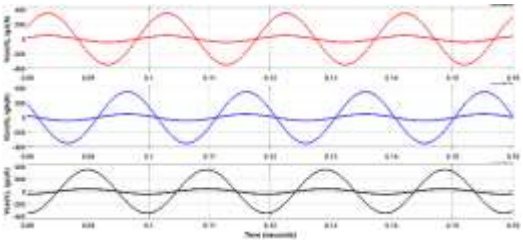


Fig. 5. illustrates the input phase voltages $(V_{an'}V_{bn'}V_{cn})$and the corresponding grid currents $(I_{ga'}I_{gb'}I_{gc})$.

The three-phase AC charging operation through the on-board Type-2 charger is carried out at a rated power of 19.4 kW. The phase currents are observed to be sinusoidal and in phase with their respective phase voltages, confirming unity power factor (UPF) operation of the Type-2 on-board charger. This validates the proper operation of the synchronous reference frame (SRF) control strategy under AC charging conditions and establishes a stable baseline for subsequent combined charging operation.

Case2: IDC Operation and Interleaving Performance

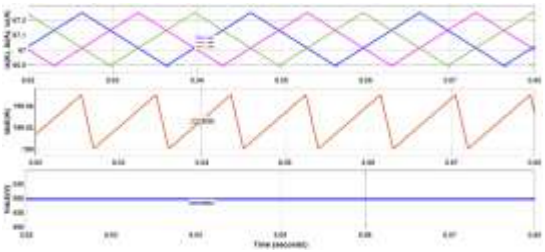


Fig. 6. Shows the inductor currents of the three inverter legs $(i_{a'}i_{b'}i_c)$, DC input current i_{dcE}, external DC source voltage V_{dcE}.

The switching behavior and current sharing of the drivetrain-integrated interleaved DC–DC converter (IDC) under DC charging operation are presented in Fig. 6. The top trace shows the inductor currents of the three inverter legs $(i_{a'}i_{b'}i_c)$, which are phase-shifted by 120° as a result of the interleaved PWM (IPWM) control strategy. This confirms balanced current sharing among the inverter legs. The middle trace represents the resultant DC input current i_{dcE}, which exhibits significantly reduced ripple compared to individual phase currents. This ripple reduction is achieved due to the interleaving effect as well as the relatively high leakage inductance of the EV motor stator windings reused as filter inductors. The bottom trace in Fig. 6 shows the external DC source voltage V_{dcE}, which remains within the permissible operating range during the charging process. The DC current reference, generated based on the proposed control law, ensures that the power drawn from the external DC source remains within acceptable limits.

Case3: Combined AC–DC Charging and DC-Link Voltage Regulation

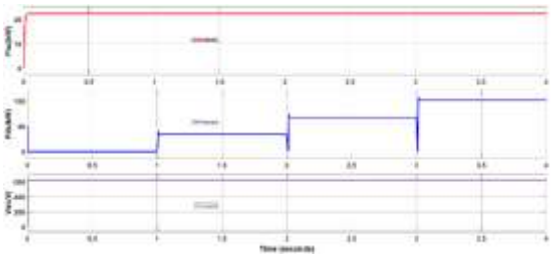


Fig. 7. Simulation results during combined AC–DC charging: average power supplied by the Type-2 on-board charger P_{ac}(top trace), power transferred through the drivetrain-integrated IDC P_{dc}(middle trace), and regulated DC-link voltage V_{dc}(bottom trace).

Fig. 7 presents the dynamic performance of the proposed combinatory AC–DC charging scheme in terms of power

contribution from the AC charger and the IDC, along with the DC-link voltage regulation. The top trace shows the AC charging power P_{ac}, which is maintained at 19.4 kW throughout the simulation. The middle trace shows the DC power contribution P_{dc} from the IDC. For the initial 1s, the DC power is intentionally maintained at zero to demonstrate AC-only charging operation, resulting in a charging rate of approximately 0.4 C. Subsequently, the IDC current reference is increased in discrete steps corresponding to charging rates of 0.56 C, 1.18 C, and 1.6 C. This staged increase demonstrates the capability of the proposed system to dynamically scale the charging power by simultaneously utilizing AC and DC sources. The bottom trace of Fig. 7 shows the DC-link voltage V_{dc}, which remains tightly regulated at its reference value despite sudden changes in DC charging power. The absence of overshoot or oscillations in the DC-link voltage clearly demonstrates the superior dynamic performance of the proposed ANFIS-based DC-link controller. Unlike a conventional PI controller, the ANFIS controller effectively compensates for system nonlinearities and coupling effects between the AC charger and IDC, thereby preventing circulating currents and ensuring stable operation during combined charging.

Case4: Battery Charging Performance with ANFIS Control

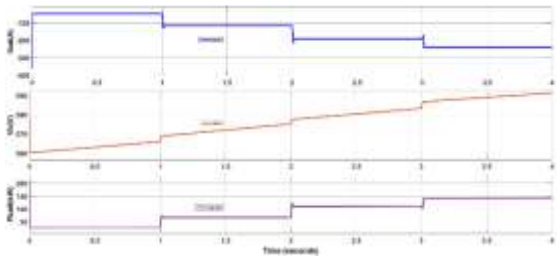


Fig. 8. Simulation results during combined AC–DC charging: battery charging current I_{bt}(top trace), battery terminal voltage V_b(middle trace), and battery charging power P_{bat}(bottom trace).

The battery charging characteristics under combined AC–DC charging was shown in Fig. 8. The top trace shows the battery charging current I_{bt}, which increases proportionally with the stepwise increase in IDC power contribution. The middle trace shows the battery terminal voltage V_b, which increases smoothly without abrupt transients, indicating safe charging operation. The bottom trace shows the battery charging power P_{bat}, which reflects the combined contribution of the AC charger and the IDC. The smooth transition in battery current and power during step changes in charging rate highlights the effectiveness of the ANFIS-based controller in managing fast dynamic interactions among multiple power sources. The adaptive nature of the ANFIS controller enables rapid adjustment of the battery-side DC–DC converter current reference, ensuring stable DC-link voltage regulation and improved charging response compared to conventional linear controllers.

CONCLUSION

This paper presented a combinatory AC–DC charging approach for electric vehicles, enabling simultaneous utilization of an on-board Type-2 AC charger and a drivetrain-integrated DC charging interface. A new DC input port, formed using the neutral point of the EV motor windings and the negative rail of the drivetrain inverter, allows the EV to accept

power from external DC sources such as renewable energy systems and DC microgrids. The drivetrain inverter was reconfigured as an interleaved DC–DC converter, with the motor stator windings acting as filter inductors. This configuration supports flexible operation under AC-only, DC-only, and combined AC–DC charging modes, allowing scalable charging rates depending on source availability. An ANFIS-based DC-link controller was implemented in MATLAB/Simulink to regulate the DC-link voltage under simultaneous multi-source charging. Simulation results demonstrated that the ANFIS controller effectively handles system nonlinearities and dynamic interactions between the AC charger and the integrated DC–DC converter. Stable DC-link voltage regulation, reduced transient disturbances, and smooth battery charging profiles were achieved even during step changes in charging power. The MATLAB/Simulink simulations validated the feasibility and effectiveness of the proposed combinatory AC–DC charging strategy. Unity power factor was achieved during AC charging, interleaved operation of the DC–DC converter reduced current ripple, and battery current and voltage profiles confirmed safe and efficient charging. These results indicate that the proposed approach provides a reliable method for faster and more flexible EV charging using hybrid AC–DC power sources.

REFERENCES

[1] M. Ehsani, Y. Gao, S. Longo, and K. E. Gay, *Modern Electric, Hybrid Electric, and Fuel Cell Vehicles*, 3rd ed. Boca Raton, FL: CRC Press, 2018.

[2] R. Xiong, H. He, F. Sun, and Y. Li, "Battery management systems for electric vehicles," *IEEE Trans. Veh. Technol.*, vol. 68, no. 7, pp. 6503–6517, Jul. 2019.

[3] T Sree Lakshmi, N Balavenkata Muni, K Meenendranath Reddy, published a paper, "Block chain enabled Secure Communication Framework for V2V and V2I Systems", in CUESTIONES DE FISIOTERAPIA, ISSN: 1135-8599, Volume 54, Issue 2, page no-1466-1474, 2025.

[4] J. Cao, Y. Zhang, and W. Su, "Fast charging technologies for electric vehicles: A review," *IEEE Trans. Power Electron.*, vol. 36, no. 3, pp. 2497–2514, Mar. 2021.

[5] P. C. Loh, D. Li, and F. Blaabjerg, "Drive-train integrated bidirectional EV chargers," *IEEE Trans. Ind. Electron.*, vol. 62, no. 12, pp. 7802–7813, Dec. 2015.

[6] R. Roopa Sri, & K. Meenendranath Reddy. (2023). Improved Power Management Control of a Multiport Converter Based EV Charging Station with PV and Battery. *International Journal of Research in Science & Engineering* , *3*(02), 16–25.

[7] Suhasnadh Reddy Veluru, Sai Teja Erukude, and Viswa Chaitanya Marella. 2025. Multimodal Detection of Fake Reviews using BERT and ResNet-50. In 2025 4th International Conference on Innovative Mechanisms for Industry Applications (ICIMIA). IEEE, 877–882.

[8] K. Tan, Y. Li, and J. Sun, "Adaptive neuro-fuzzy control for DC-link voltage regulation in EV charging systems," *IEEE Trans. Ind. Electron.*, vol. 64, no. 6, pp. 4957–4967, Jun. 2017.

[9] Cyril, H. P. (2025). Event-Driven Provisioning Architectures For Modern Telecom Networks: Overcoming Legacy Limitations And Enabling Autonomous 6g Operations. International Journal of Advanced Research in Computer Science,

16(6), 75–82. https://doi.org/10.26483/ijarcs.v16i6.7389.
[10] J. Rodriguez, S. Bernet, B. Wu, J. O. Pontt, and S. Kouro, "Multilevel voltage-source-converter topologies for industrial medium-voltage drives," *IEEE Trans. Ind. Electron.*, vol. 54, no. 6, pp. 2930–2945, Dec. 2007.
[11] Jay Bharat Mehta. (2025). AUTONOMOUS PATCH VALIDATION FOR ZERO-DAY EXPLOITS IN ENTERPRISE CLOUDS. International Journal of Applied Mathematics, 38(4s), 1270–1285. https://doi.org/10.12732/ijam.v38i4s.685.
[12] Poojari, R. (2025). A Comparative Analysis of Fine-Tuning Versus Retrieval-Augmented Approaches for Enhancing Healthcare-Centric Large Language Models.
[13] R. Krishnan, *Electric Motor Drives: Modeling, Analysis, and Control*, 2nd ed. Upper Saddle River, NJ: Prentice Hall, 2001.
[14] P Reddy, S. K. R. (2025). Tailoring Loyalty Rewards Systems across Industries: Cloud vs On-Prem Solutions. International Journal of All Research Education and Scientific Methods (IJARESM).
[15] S. Haykin, *Neural Networks and Learning Machines*, 3rd ed. Upper Saddle River, NJ: Pearson, 2009.
[16] Balavenkata Muni, N., Sasikumar, S., Hussain, K., Reddy, K.M. (2022). A Progressive Approach of Designing and Analysis of Solar and Wind Stations Integrated with the Grid Connected Systems. In: Kalinathan, L., R., P., Kanmani, M., S., M. (eds) Computational Intelligence in Data Science. ICCIDS 2022. IFIP Advances in Information and Communication Technology, vol 654. Springer, Cham.
[17] L. A. Zadeh, "Fuzzy sets," *Inf. Control*, vol. 8, no. 3, pp. 338–353, 1965.
[18] K.Meenendranath Reddy, & Syed Reshma. (2022). A Comparative Analysis of Integrated DC Microgrid with Hybrid Power Generation Systems by an Intelligent Control Strategy. International Journal of Recent Research in Electrical and Electronics Engineering, 9(2), 1–10.
[19] D. S. Kirschen and G. Strbac, *Fundamentals of Power System Economics*, 2nd ed. Hoboken, NJ: Wiley, 2018.